RESEARCH ARTICLE

microRNA Regulatory Network Inference Identifies miR-34a as a Novel Regulator of TGF-β Signaling in Glioblastoma

Giannicola Genovese[1,4], Ayla Ergun[2], Sachet A. Shukla[1,6], Benito Campos[1,7], Jason Hanna[8], Papia Ghosh[1], Steven N. Quayle[1], Kunal Rai[1,4], Simona Colla[1,4], Haoqiang Ying[1,4], Chang-Jiun Wu[1,4], Sharmistha Sarkar[1,4], Yonghong Xiao[1], Jianhua Zhang[1,5], Hailei Zhang[1,9], Lawrence Kwong[1,4], Katherine Dunn[1], Wolf Ruprecht Wiedemeyer[10], Cameron Brennan[11], Hongwu Zheng[1,12], David L. Rimm[8], James J. Collins[2,3], and Lynda Chin[1,4,5,9]

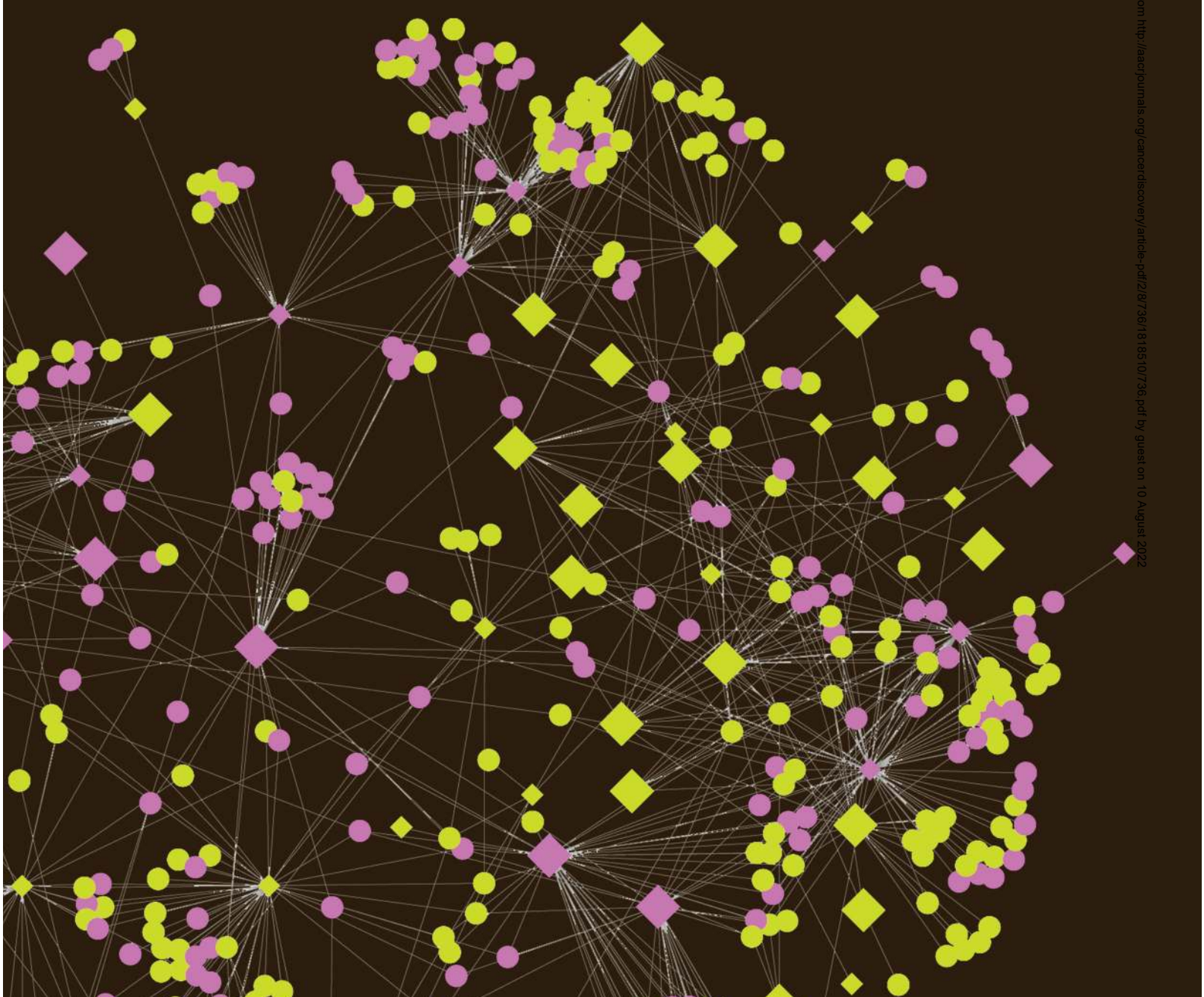

ABSTRACT

Leveraging The Cancer Genome Atlas (TCGA) multidimensional data in glioblastoma, we inferred the putative regulatory network between microRNA and mRNA using the Context Likelihood of Relatedness modeling algorithm. Interrogation of the network in context of defined molecular subtypes identified 8 microRNAs with a strong discriminatory potential between proneural and mesenchymal subtypes. Integrative *in silico* analyses, a functional genetic screen, and experimental validation identified miR-34a as a tumor suppressor in proneural subtype glioblastoma. Mechanistically, in addition to its direct regulation of platelet-derived growth factor receptor-alpha (*PDGFRA*), promoter enrichment analysis of context likelihood of relatedness–inferred mRNA nodes established miR-34a as a novel regulator of a *SMAD4* transcriptional network. Clinically, miR-34a expression level is shown to be prognostic, where miR-34a low-expressing glioblastomas exhibited better overall survival. This work illustrates the potential of comprehensive multidimensional cancer genomic data combined with computational and experimental models in enabling mechanistic exploration of relationships among different genetic elements across the genome space in cancer.

SIGNIFICANCE: We illustrate here that network modeling of complex multidimensional cancer genomic data can generate a framework in which to explore the biology of cancers, leading to discovery of new pathogenetic insights as well as potential prognostic biomarkers. Specifically in glioblastoma, within the context of the global network, promoter enrichment analysis of network edges uncovered a novel regulation of TGF-β signaling via a Smad4 transcriptomic network by miR-34a. *Cancer Discov; 2(8); 736–49. ©2012 AACR.*

INTRODUCTION

Glioblastoma is the most common primary brain tumor in adults. Patients with newly diagnosed glioblastoma have a median survival of 12 months with generally poor responses to chemoradiotherapy (1). Recent genome-wide profiling studies have shown extensive genetic heterogeneity among glioblastoma samples with distinct molecular subtypes; that these transcriptomic subtypes reflect distinct underlying biology is supported by observed differences in clinical outcome of the patients (2, 3), enrichment of different genomic and epigenetic alterations within each subtype, and differential activation of major signaling pathways (4, 5).

Noncoding RNAs have emerged as an important class of regulatory molecules in both normal and neoplastic development. MicroRNA (or miR) is a class of noncoding small RNAs produced by RNA polymerase II as hairpins of longer precursor RNAs that are subsequently processed to approximately 22-nt-long fragments by RNase III enzymes, Drosha and Dicer. Mature miRs regulate gene expression by promoting mRNA degradation or by inhibiting mRNA translation (6, 7). The connection between miRs and cancer was first implicated by their genomic alteration and dysregulated expression in various human tumors (8–12). Multiple miRs have since been identified to promote or suppress oncogenesis in various tumors, presumably by modulating gene expression in the oncogenic and tumor suppressor networks. In addition, recent studies have proposed new mechanisms of miR–mRNA regulation such as modulation of mRNA with competitive miR-binding sites (sponge interactions) or mRNAs that affect constituents of the miR regulatory machinery (nonsponge interactions; refs. 13–15).

Global views of the relationship between miR and mRNA expression have been reported. For instance, Su and colleagues (16) used integrative genomics and genetic techniques to characterize the roles of mouse miRs within the mouse liver miR–mRNA network; Dong and colleagues (17) deciphered the pathway connecting mutations under the glioblastoma miR–mRNA expression network; Mestdagh and colleagues (18) established the miR body map online resource to dissect miR function through integrative genomics; Grigoryev and colleagues (19) presented the genome-wide

Authors' Affiliations: [1]Department of Medical Oncology, Dana-Farber Cancer Institute; [2]Howard Hughes Medical Institute, Department of Biomedical Engineering and Center for BioDynamics, Boston University; [3]Wyss Institute for Biologically Inspired Engineering, Harvard University, Boston, Massachusetts; [4]Department of Genomic Medicine, [5]Institute for Applied Cancer Science, MD Anderson Cancer Center, Houston, Texas; [6]Department of Statistics, Iowa State University, Ames, Iowa; [7]Division of Neurosurgical Research, Department of Neurosurgery, Heidelberg University, Heidelberg, Germany; [8]Department of Pathology, Yale University Medical School, New Haven, Connecticut; [9]The Eli and Edythe L. Broad Institute of Massachusetts Institute of Technology and Harvard University, Cambridge, Massachusetts; [10]Women's Cancer Program at the Samuel Oschin Comprehensive Cancer Institute, Cedars Sinai Medical Center, Los Angeles, California; [11]Department of Neurosurgery, Memorial Sloan-Kettering Cancer Center; and [12]Cold Spring Harbor Laboratory, Cold Spring Harbor, New York

Note: Supplementary data for this article are available at Cancer Discovery Online (http://cancerdiscovery.aacrjournals.org/).

G. Genovese, A. Ergun, and S.A. Shukla contributed equally to this work.

Corresponding Authors: Lynda Chin, MD Anderson Cancer Center, 1901 East Road, Rm 4SCR6.2080, Houston, TX 77054. Phone: 713-792-6876; Fax: 713-92-6806; E-mail: LChin@mdanderson.org, and James J. Collins, jcollins@engc.bu.edu

doi: 10.1158/2159-8290.CD-12-0111

miR regulation of T-lymphocyte activation through the mapped miR, mRNA, and protein networks; and Sharbati and colleagues (20) studied macrophage infection via an integrated miR–mRNA network. In these global integrative miR–mRNA network analyses, either general correlation coefficient methods (16–18) or putative miR target prediction methods (19, 20) have been used to construct or map miR–mRNA connections. These approaches preferentially quantify linear dependencies between pairwise variables.

Recognizing that the functional relationship between 2 variables in cancer is not necessarily linear, we explored a mutual information–based approach in this work that scores miR–mRNA interaction strength on the basis of relevant expression contexts. This mutual information–based approach has been used recently by Sumazin and colleagues (13) to uncover a novel class of modulators of miR–mRNA interactions. Here, we applied the Context Likelihood of Relatedness (CLR; ref. 21) network modeling algorithm to generate pairwise measures of associations on the basis of mutual information through calculation of the entropy. At the heart of the CLR algorithm is a unique statistical background correction test which uses the full set of mutual information values to estimate a significance value for each miR–mRNA pair under a given observed network context (see Supplementary Information). The algorithm evaluates the mutual information value of a miR–mRNA pair against the background mutual information distribution of all mRNAs in the data set with the miR, as well as with the distribution of mutual information values of all miRs with the mRNA under consideration. A combined *z*-score summarizing these 2 comparisons is generated, and the list of all such pairwise *z*-scores is subsequently used to generate *P* values by comparing with the normal distribution. A stringent false discovery rate of 5% is finally applied to identify putative miR–mRNA regulatory edges. Interactions whose mutual information values are outliers in the right tails of the pertinent context background distributions of mutual information scores have the greatest likelihood of being identified as significant. This background correction method allows the CLR algorithm to filter out those edges between miRs and mRNA that have spurious similarities with large numbers of other gene–miR species.

The Cancer Genome Atlas (TCGA) has characterized the genomes of glioblastoma on multiple dimensions including coding and noncoding RNAs (22). We applied the CLR modeling algorithm to this multidimensional data set to infer putative regulatory relationships (edges) between miRs and mRNAs in glioblastoma. Specifically, we were interested in directional miR–mRNA interactions where the miR downregulates mRNA expression either directly through binding or indirectly through intermediary effectors. Against this global network, we explored the functional relationship between miRs and mRNAs in gliomagenesis.

RESULTS

Global miR and mRNA Regulatory Network in Glioblastoma

To explore the relationship between miRs and mRNAs, we applied the CLR network algorithm to miR and mRNA transcriptome data from 290 glioblastoma samples from the TCGA (Supplementary Table S1). A total of 26,297 edges between 254 miR and 6,152 mRNA nodes were defined (Supplementary Table S2). Next, we integrated genome-wide copy number profiles with the inferred edges of the network with the assumption that biologically relevant miRs or mRNAs are likely to show additional levels of dysregulation across the samples. Here, we found that a third (34.1%) of the miR nodes or mRNA nodes in the CLR network resided in regions of copy number aberration in glioblastoma and 3.9% involved both miR and mRNA that are localized in regions of genomic alterations (Fig. 1A and B). This integrative analysis thus prioritized 1,018 edges involving 69 miRs and 467 mRNAs nodes as candidates with likely biologic importance.

To further rank the above nodes, we next applied a putative direct-target filter. Specifically, on the basis of previous findings showing that miRs downregulate their target mRNAs by binding to their 3′-untranslated regions (UTR; ref. 6), we defined a subset of mRNA nodes as putative direct targets of their miR nodes on the basis of the following parameters: (i) a significant negative correlation (Pearson correlation coefficient ≤ -0.3) between expression of miR and mRNA and (ii) sequence-based prediction of interaction in all 3 sequence-based prediction databases, namely, PicTar, TargetScan, and miRanda (23–27). This *in silico* analysis identified 3 edges involving 6 of the 536 prioritized nodes as representing putative direct interactions, namely, miR-34a:*PDGFRA*; mir-27a:*CPEB3*; and miR-23a:*ARHGEF7*. The same trend is observed with the global CLR network edges, where 45 (0.17%) of the 26,297 CLR-inferred edges were predicted computationally to be direct (Fig. 1C; Supplementary Table S3). This suggests that a significant proportion of the putative miR–mRNA relationships may be indirect, possibly mediated via intermediaries such as transcription factors (see below).

Functional Analyses of Subtype-Discriminant miR Nodes

Next, we asked whether the CLR-inferred global network captures the salient transcriptomic features of the 4 molecular subtypes of glioblastoma. Here, we looked for edges that are unique to each molecular subtype (Supplementary Table S4) as well as differential expression of the miR and mRNA nodes between any 2 molecular subtypes. We found that the variability among molecular subtypes appeared to be the predominant driver of relationships defined by CLR (Supplementary Fig. S1). For example, 67% (n = 17,934) of the network edges involved miR and mRNA that are differentially expressed ($P < 0.001$) between 2 molecular subtypes. While the difference in expression between the subtype signature genes is not surprising, it is striking that the CLR-identified miRs associated with these genes show a reciprocal and opposite change of expression along with their mRNA nodes. In particular, the greatest transcriptomic shift was observed between proneural and mesenchymal subtypes with nearly half of the edges in the global network (or 12,673 edges, 48%) marked by expression differences between them. This observation suggested that miR regulation of mRNA may play a role in defining the molecular signatures of these 2 subtypes. To this end, we looked for CLR-inferred edges among the 685 significantly overexpressed genes used by Verhaak and colleagues (3) for subtype pathway/

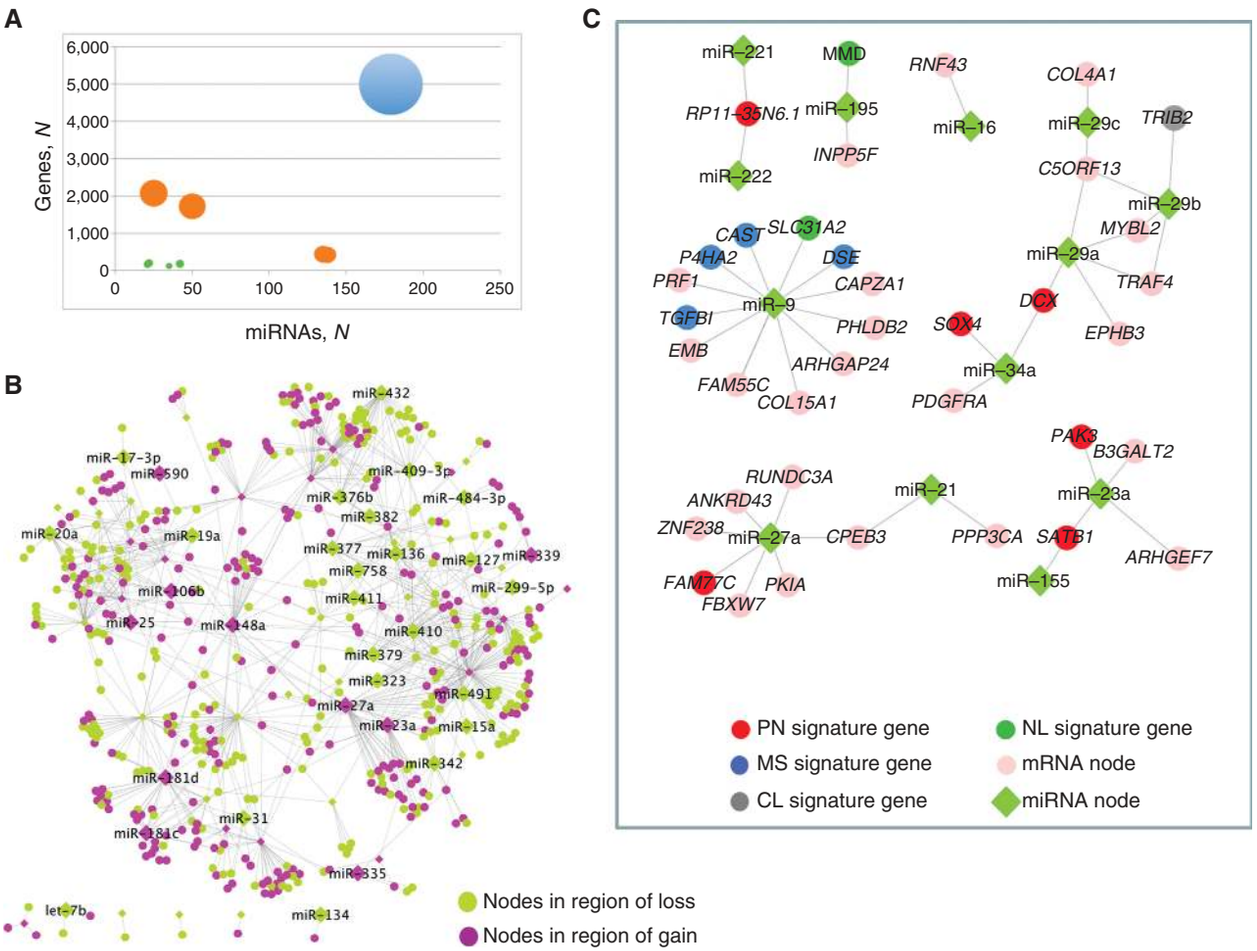

Figure 1. Integrative analyses of CLR network in context of copy number alterations and direct target prediction. **A,** CLR network grouped by connectivity among miRs and mRNAs in regions of copy number aberration. Size of the node represents the number of edges between the miR and mRNAs in each group. There are 9 subnetworks represented. Edges in the network where both participating miR and mRNA are in regions of copy number alterations account for less than 3.9% of the total connectivity (green circles). Edges where either the participating miR or the mRNA is in region of gain or loss, but not both, account for 34.1% of the network (orange circles). Approximately 62% of the network involves miRs and mRNAs without evidence of genomic alterations in glioblastoma (blue circle). **B,** network of CLR edges where both miR (diamonds) and mRNA (circles) are in regions of copy number gain (purple nodes) or loss (green nodes). **C,** putative direct-target subnetworks among CLR-identified edges in glioblastoma. miRs are represented as green diamonds and genes as circles; classical signature genes (gray), neural signature genes (dark green), proneural signature genes (red), mesenchymal signature genes (blue), genes not in any of the molecular subtype signatures (pink). CL, classical; MS, mesenchymal; NL, neural; PN, proneural.

Gene Ontology (GO) enrichment analysis. Of these 685 genes, 506 of them (73%) have inferred edges to a miR node in the global CLR network. Conversely, of the 2,984 inferred edges to these 506 subtype classifier genes, a disproportionate number (70%) are part of either the proneural or mesenchymal subtype signatures (e.g., 328 to classical, 560 to neural, 858 to proneural, and 1,238 to mesenchymal signature genes), suggesting that miR–mRNA regulation may contribute to gene signatures underlying these 2 molecular subtypes. Indeed, 8 miR nodes ($P < 0.001$) were found to be highly discriminatory between proneural and mesenchymal subtypes (Fig. 2A; see Supplementary Methods). Five of these miR nodes (miR-22, miR-34a, miR-223, miR-142-3p, and miR-142-5p) are underexpressed in proneural-subtype glioblastomas, harboring inferred negative edges with proneural signature genes; conversely, 3 of them (miR-9, miR-181c, and miR-181d) are underexpressed in mesenchymal-subtype glioblastoma with inferred negative edges with mesenchymal signature genes (Fig. 2B). When integrated with copy number and expression profiles as well as putative direct-target prediction as above (Supplementary Table S5), we found that miR-34a is the only one that also resides in a region of frequent loss and harbors a putative direct CLR edge to *PDGFRA* (platelet-derived growth factor receptor-alpha), a well-known proneural signature gene that is also a target of genomic amplification.

Next, we sought evidence that these 8 miRs are functionally active in a proneural context. Recognizing the limitation of established cell systems in modeling proneural molecular subtype, we first investigated whether a genetically engineered mouse (GEM) model of glioblastoma constructed with concomitant *p53* and *Pten* deletion in neural stem cells (NSC) and neural progenitors (*Gfap-Cre;p53*$^{L/L}$*;Pten*$^{L/+}$) can be considered an appropriate model of proneural glioblastoma (28). Here, we conducted gene set enrichment analysis

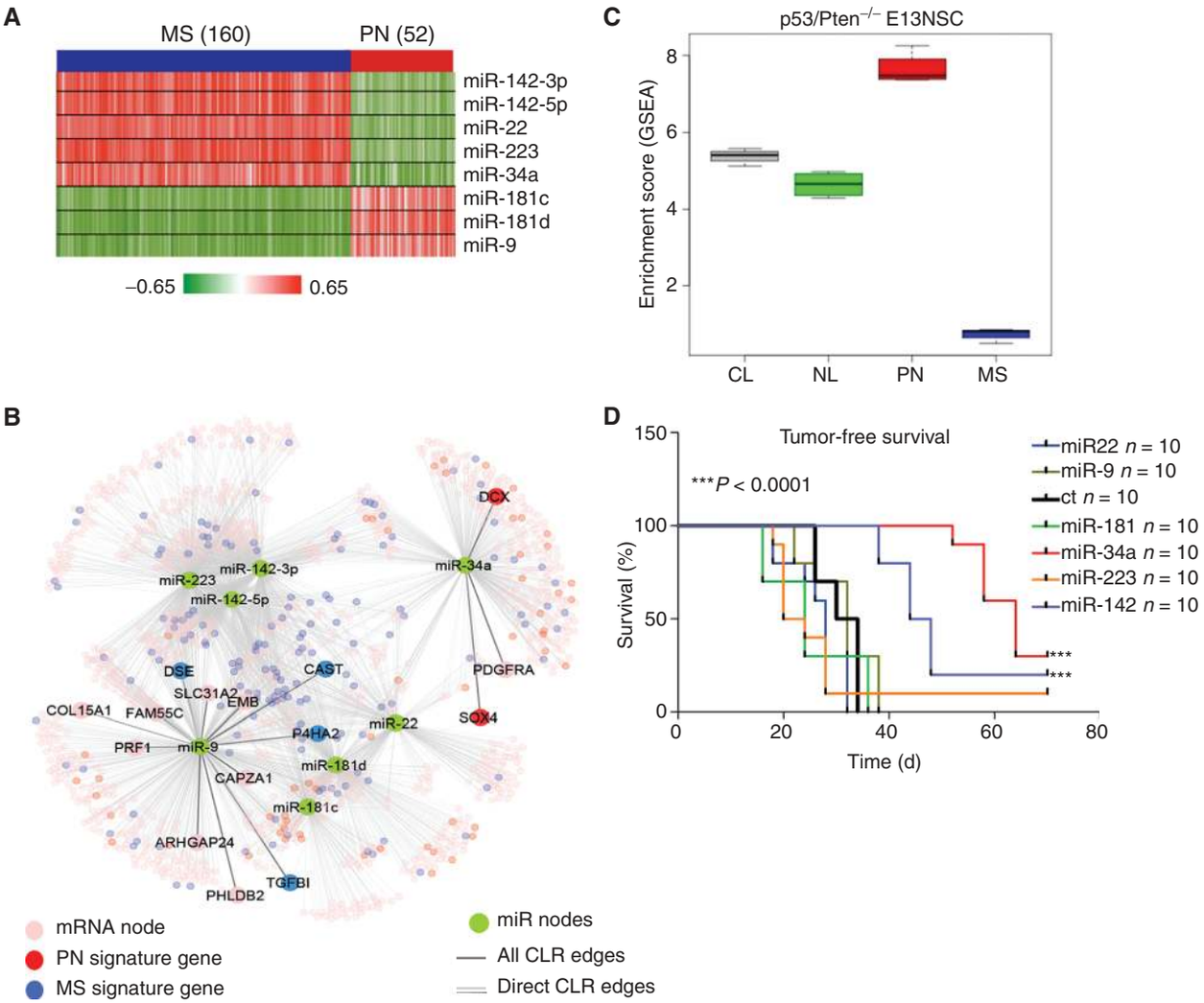

Figure 2. Discriminatory miRs between proneural and mesenchymal subtypes. **A,** heatmap of correlations between 8 most discriminative miRs with proneural (PN) and mesenchymal (MS) signature genes in the CLR network. Each cell in the heatmap is the correlation between the corresponding miR and signature gene across samples. **B,** CLR network around the 8 miRs with putative direct targets highlighted. **C,** GSEA of premalignant spheroid cultures derived from *p53/Pten*$^{-/-}$ E13 mouse embryos (*p53*$^{L/L}$;*Pten*$^{L/L}$;*Gfap-Cre*). For any subtype signature gene list, the enrichment of the subtype in a given sample is calculated by comparing the average expression of the signature genes with the overall mean using a *t*-statistic. Each box plot in the figure encapsulates the distribution of these subtype enrichment scores across all samples for the individual subtypes. A clear enrichment is observed for proneural signature genes ($P = 3.66 \times 10^{-12}$, $n = 4$). CL, classical; NL, neural. **D,** Kaplan–Meier survival analysis of Ncr/nude mice transplanted subcutaneously with premalignant proneural-like *p53/Pten*$^{-/-}$ NSCs transduced with 6 pre-miRs corresponding to 8 discriminant miRs or the GFP control ($n = 10$ per group). miR-34a and miR-142 potently impaired tumorigenesis when compared with GFP control (***, $P < 0.0001$). ct, control.

(GSEA; ref. 29) of the transcriptomes of premalignant *p53/Pten* double-null E13 embryonic NSC (*Gfap-Cre;p53*$^{L/L}$;*Pten*$^{L/L}$) and tumor spheroids isolated from malignant gliomas developed in the context of *p53* and *Pten* deficiency (*Gfap-Cre;p53*$^{L/L}$;*Pten*$^{L/+}$; Supplementary Fig. S2A). As shown in Fig. 2C and Supplementary Fig. S2B, significant enrichments for the proneural signature genes were observed in both premalignant embryonic NSCs and in malignant tumor spheroids ($P = 3.66 \times 10^{-12}$ and $P = 2.2 \times 10^{-16}$, respectively), thus substantiating the *p53/Pten* double-null model as a proneural model. Next, we enforced expression of the miR precursors corresponding to the 8 subtype discriminant miRs in premalignant *p53/Pten*$^{-/-}$ NSCs (Supplementary Fig. S3). As summarized in Fig. 2D, both miR-34a and miR-142 significantly inhibited tumorigenesis of *p53/Pten*$^{-/-}$E13 NSCs *in vivo*, suggesting tumor-suppressive activity in this context. In summary, subtype-discriminant miRs are functionally active in proneural glioblastoma context.

miR-34a Expression Is Prognostic in Glioblastoma

To explore the potential clinical relevance of subtype-discriminant miRs in human glioblastoma, we asked whether their expression tracks with any clinical parameters, particularly prognosis (see Methods). As summarized in Supplementary Table S6, when dichotomized, miR-34a expression was the only 1 of the 8 miRs that showed significant prognostic correlation (Bonferroni-adjusted, $P = 0.0047$) in the TCGA data set. Specifically, patients with miR-34a low-expressing glioblastomas exhibited an overall improved survival (Fig. 3A).

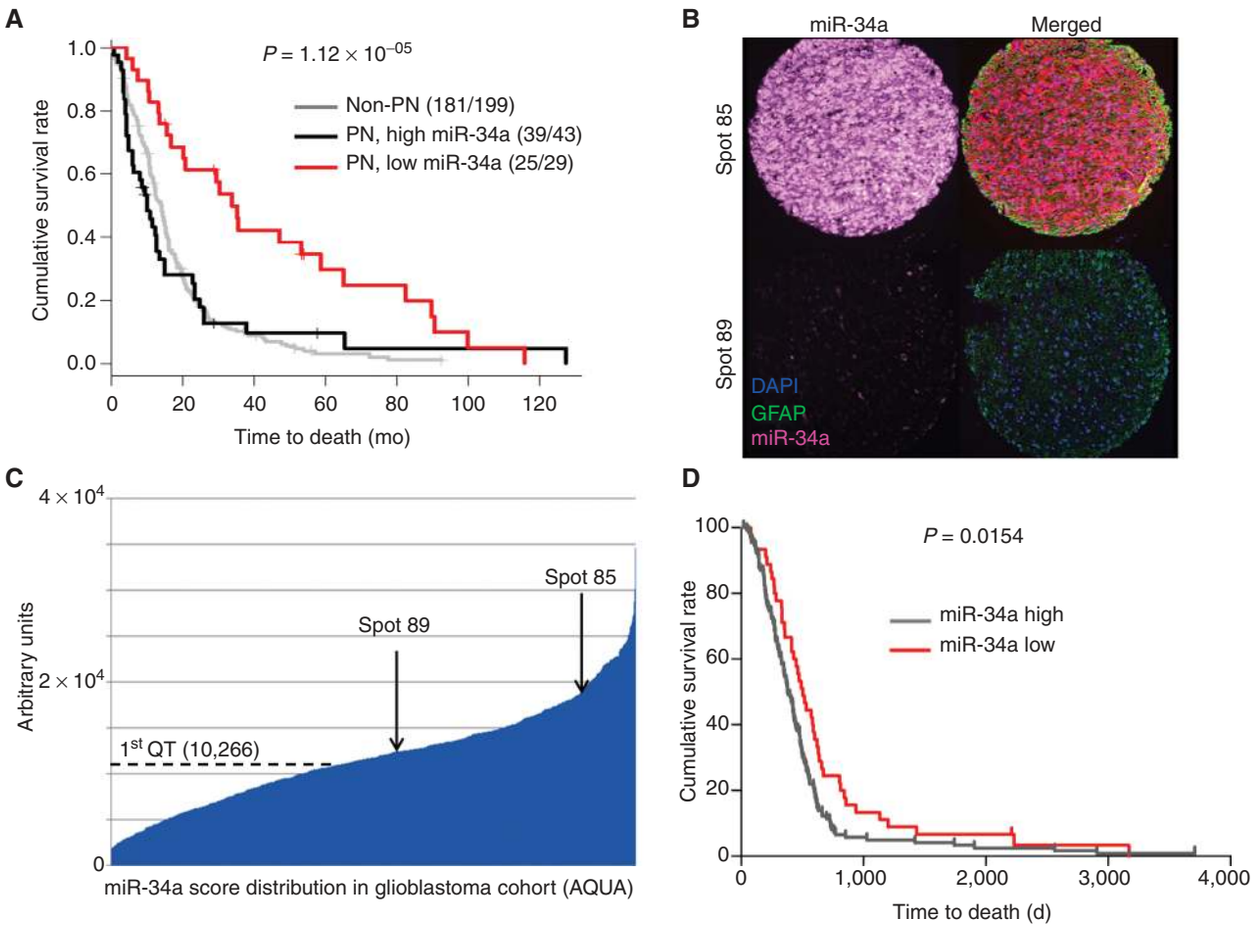

Figure 3. miR-34a levels are prognostic in glioblastoma. **A,** Kaplan–Meier survival analysis of patients in the TCGA data set ($n = 271$). Low expression of miR-34a stratifies a subgroup of patients with proneural (PN) glioblastoma with a significant survival advantage compared with others in TCGA cohort (log-rank $P = 1.12 \times 10^{-5}$). **B,** glioblastoma tissue microarray. Representative spots showing high and low expressors. A locked nucleic acid–modified probe for miR-34a and an antibody specific for glial fibrillar acidic protein (GFAP) were hybridized to the arrays. **C,** Automated Quantitative Analysis (AQUA) score distribution across the glioblastoma cohort. Arrows indicate the AQUA score for the samples shown in **B.** QT, quartile. **D,** Kaplan–Meier survival analysis of patients in the independent training cohort ($n = 220$). Subjects were stratified in high and low miR-34a expressors based on the quantile expression assessed by the AQUA score. First (lower) quartile of the AQUA score distribution was used as cutoff to assign patients to the low or high expressors groups. "miR-34a low" patients show a significant better outcome than "high expressors" ($P = 0.0154$).

Moreover, miR-34a low expression did not simply identify the proneural subtype, which is known to have better outcome (2, 3). Instead, within the proneural subtype, low miR-34a expression stratifies a subgroup of patients with proneural glioblastoma with improved overall survival (HR, 2.2; $P = 2.2E-05$), compared with miR-34a high-expressing proneural patients or other non-proneural patients (Supplementary Table S6); moreover, the prognostic significance of miR-34a was independent from other clinical variables such as therapy and gender or batches in multivariate analyses (Supplementary Table S7).

Importantly, this prognostic correlation of miR-34a was recapitulated in an independent cohort of human glioblastoma. Briefly, we conducted quantitative *in situ* hybridization using miR-34a as probe on a tissue microarray from an independent cohort of human gliomas (Fig. 3B and C; Supplementary Fig. S4 and Supplementary Tables S8 and S9) and showed that low miR-34a expressors were indeed associated with better overall survival ($P = 0.0154$; Fig. 3D).

miR-34a Is a Tumor Suppressor in Proneural Glioblastoma

Its potent tumor-suppressive activity *in vivo*, evidence of genomic alteration, and its putative direct mRNA target PDGFRA, coupled with its prognostic significance, together strongly nominated miR-34a for mechanistic studies. Although it has been shown to be a tumor suppressor in multiple human cancer types including glioblastoma (30, 31), a specific role in proneural glioblastoma has not been fully shown. Similar to the pattern of lower expression in human proneural-subtype glioblastoma ($P = 1.92e-19$; Supplementary Fig. S5A), miR-34a expression was lower in *p53*/*Pten* double-null tumor spheroids or NSCs than in normal NSCs ($P = 0.0034$ and $P = 0.0036$, respectively; Supplementary Fig. S5B); moreover, the acute deletion of *p53* and *Pten* by *ex vivo* CRE expression in early-passage primary astrocytes results in significant downregulation of endogenous miR-34a

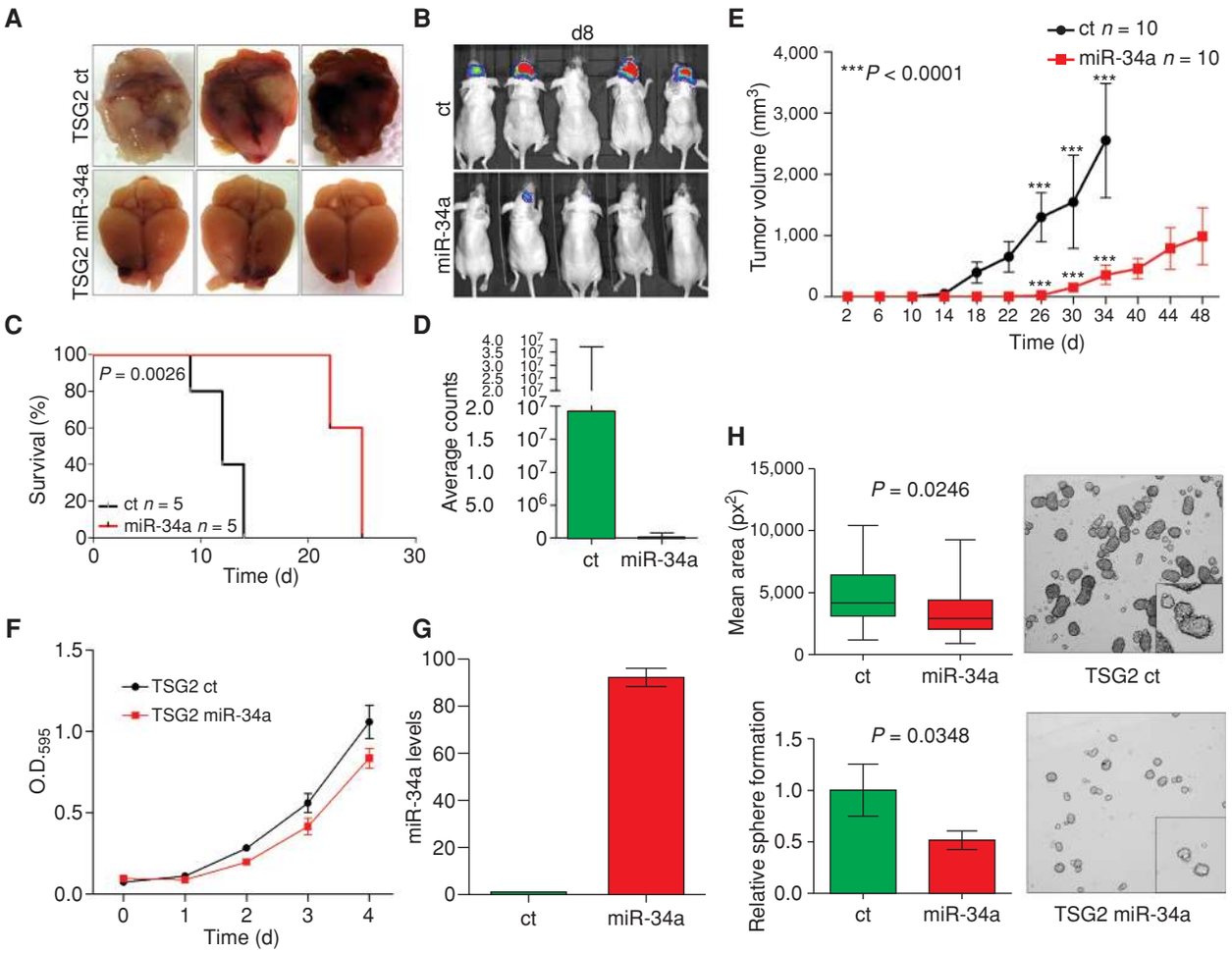

Figure 4. miR-34a regulates self-renewal and tumorigenesis in proneural glioblastoma. TSG2 cells, a proneural-like malignant cell line derived from a $p53^{L/L}$;$Pten^{L/+}$;*Gfap-Cre* mouse glioma, were coinfected with a luciferase reporter and with lentiviral particles harboring the miR-34a precursor or the control vector and injected orthotopically (frontal lobe) in Ncr/nude mice. **A,** macroscopic appearance of mouse brains injected with *p53*/$Pten^{-/-}$ glioblastoma cells harboring miR-34a or the vector control isolated from terminally ill mice. Reintroduction of miR-34a results in poorly invasive tumors confined to the frontal lobe (bottom). **B,** bioluminescence images of Ncr/nude mice transplanted orthotopically with *p53*/$Pten^{-/-}$ murine glioblastoma cells harboring a luciferase construct along with miR-34a or the vector control. Images taken 8 days after surgery show a significantly higher tumor burden in control mice. **C,** Kaplan–Meier survival analysis of Ncr/nude mice transplanted orthotopically (frontal lobe) with *p53*/$Pten^{-/-}$ glioblastoma cells harboring miR-34a or the vector control. **D,** quantification of bioluminescence imaging. Mice were imaged 8 days after surgery; the plots show a significant difference in tumor burden between control and miR-34a tumors as assessed by photon counts. Error bars represent SD of 5 experimental replicates. **E,** miR-34a impairs *in vivo* the tumorigenic potential of proneural-like TSG2 cells transplanted subcutaneously into the flanks of Ncr/nude mice. Average tumor volumes are plotted. Error bars represent the SD of experimental replicates. **F,** miR-34a does not affect cell proliferation in 2-dimensional culture. Cells were stained with crystal violet and assessed for their ability to grow *in vitro*. Error bars represent the SD of experimental replicates. O.D., optical density. **G,** expression levels of miR-34a in murine proneural-like TSG2 malignant glioma cells by reverse transcriptase-quantitative PCR 72 hours after infection with lentivirus harboring a miR-34a precursor or the control vector. Error bars represent SD of replicates. **H,** reintroduction of miR-34a in TSG2 spheroids decreases their self-renewal potential. Error bars represent extreme values (top graph) and SD of experimental triplicates (bottom graph).

($P = 0.002$; Supplementary Fig. S5C and S5D). Functionally, in TSG2, a tumor spheroid culture derived from a murine *p53*/$Pten^{-/-}$ glioblastoma, miR-34a expression significantly inhibited *in vivo* tumorigenesis in both orthotopic xenografts ($P = 0.0026$) and in subcutaneous transplants ($P < 0.0001$; Fig. 4A–E), resulting in prolonged survival of tumor-bearing mice and a less aggressive growth pattern (Supplementary Fig. S6A). While potently inhibiting tumorigenesis *in vivo*, it was interesting that miR-34a overexpression did not impact significantly on cell proliferation in 2-dimensional culture experiments (Fig. 4F and G). Although it is possible that the lack of growth phenotype may reflect the possibility that cells under the selective pressure of miR-34a overexpression may undergo negative selection *in vitro*, as observed *in vivo* in tumors arising from cells stably transduced with a miR-34a lentivector (Supplementary Fig. S6B), the phenotype of significant impairment of spherogenic potency in both human and mouse tumor neurospheres implicates renewal potential as a phenotype impacted by miR-34a expression. In particular, spherogenic renewal of murine TSG2 cultured in NSC medium in the presence of fibroblast growth factor (FGF) and epidermal growth factor (EGF) was inhibited by miR-34a expression (Fig. 4H). Similarly, this phenotype was recapitulated

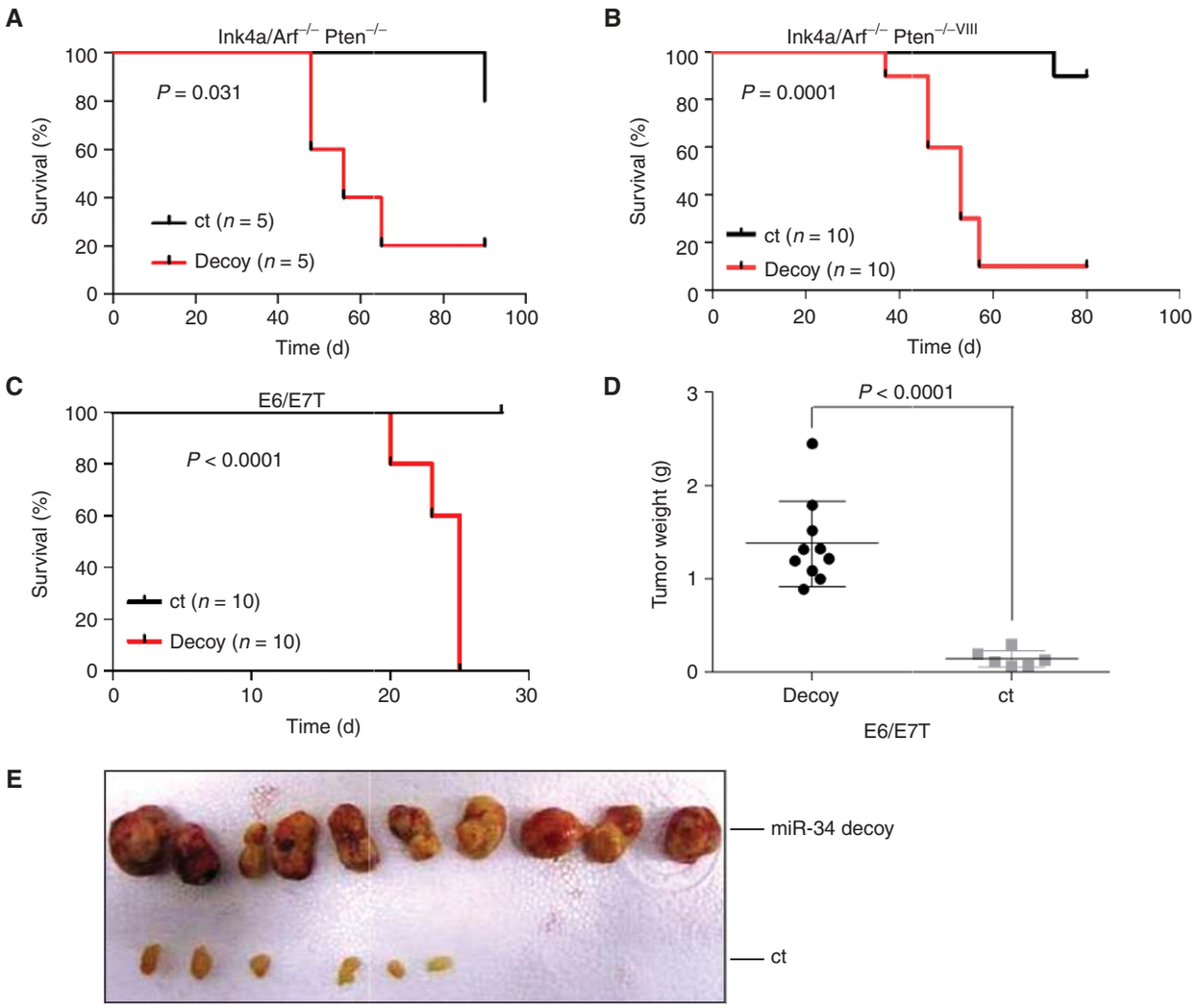

Figure 5. miR-34a knockdown transforms GEM and human astrocytes. **A** and **B,** knockdown by miR-34a decoy enhances the tumorigenic potential of *Ink4a/Arf*$^{-/-}$;*Pten*$^{-/-}$ and *Ink4a/Arf*$^{-/-}$;*Pten*$^{-/-}$;*Egfr*$^{VIII/+}$ adult mouse astrocytes *in vivo*. Kaplan–Meier analysis of tumor-free survival of Ncr/nude mice transplanted subcutaneously with decoy and control adult mouse astrocytes. **C,** Kaplan–Meier analysis of tumor-free survival of Ncr/nude mice transplanted subcutaneously with decoy and control E6/E7T human astrocytes. **D,** average weight of tumors generated by decoy and ct E6/E7T cells. Error bars represent SD of experimental replicates. **E,** macroscopic appearance of tumors generated by decoy and ct E6/E7T astrocytes.

in TS543, a human proneural-like glioblastoma spheroid showing concomitant amplification and overexpression of *PDGFRA*, upon miR-34a overexpression (Supplementary Fig. S7A and S7B).

Conversely, to show a gain-of-oncogenic function in the context of miR-34a loss, we used a decoy 3′UTR system to functionally knockdown miR-34a as previously described (32). Indeed, stable decoy expression resulted in enhanced tumorigenicity *in vivo* in human E6/E7T astrocytes and in mouse *Ink4a/Arf*$^{-/-}$;*Pten*$^{-/-}$ and *Ink4a/Arf*$^{-/-}$*Pten*$^{-/-}$;*Egfr*$^{VIII/+}$ astrocytes resulting in decreased tumor-free survival (Fig. 5A–E; Supplementary Fig. S8A and S8B). Taken together, these *in vitro* and *in vivo* functional data in mouse and human systems, both by exogenous genetic perturbation and by endogenous downregulation of miR-34a, unequivocally prove that miR-34a is a glioblastoma tumor suppressor in the proneural subtype.

miR-34a Directly Regulates *PDGFRA*

To understand its mechanism of action in proneural glioblastoma, we explored the molecular basis of miR-34a action within the context of the established CLR network. First, we focused on *PDGFRA* as the predicted direct target of miR-34a as they represent the 2 nodes of a CLR-defined edge and both are subjected to genomic alterations, in addition to *PDGFRA* being a known signature oncogene in proneural subtype of glioblastoma (2). Specifically, we looked to confirm direct binding of *PDGFRA* by miR-34a using a 3′UTR luciferase reporter assay. Indeed, the direct nature of endogenous miR-34a–*PDGFRA* interaction was validated by this assay in E6/E7T human astrocytes (Supplementary Fig. S9A). Supporting the biologic relevance of this interaction, PDGFRA expression was downregulated by enforced expression of miR-34a in 2 independent mouse (TSG1 and TSG2) and human (TS543) proneural tumor spheroid cultures

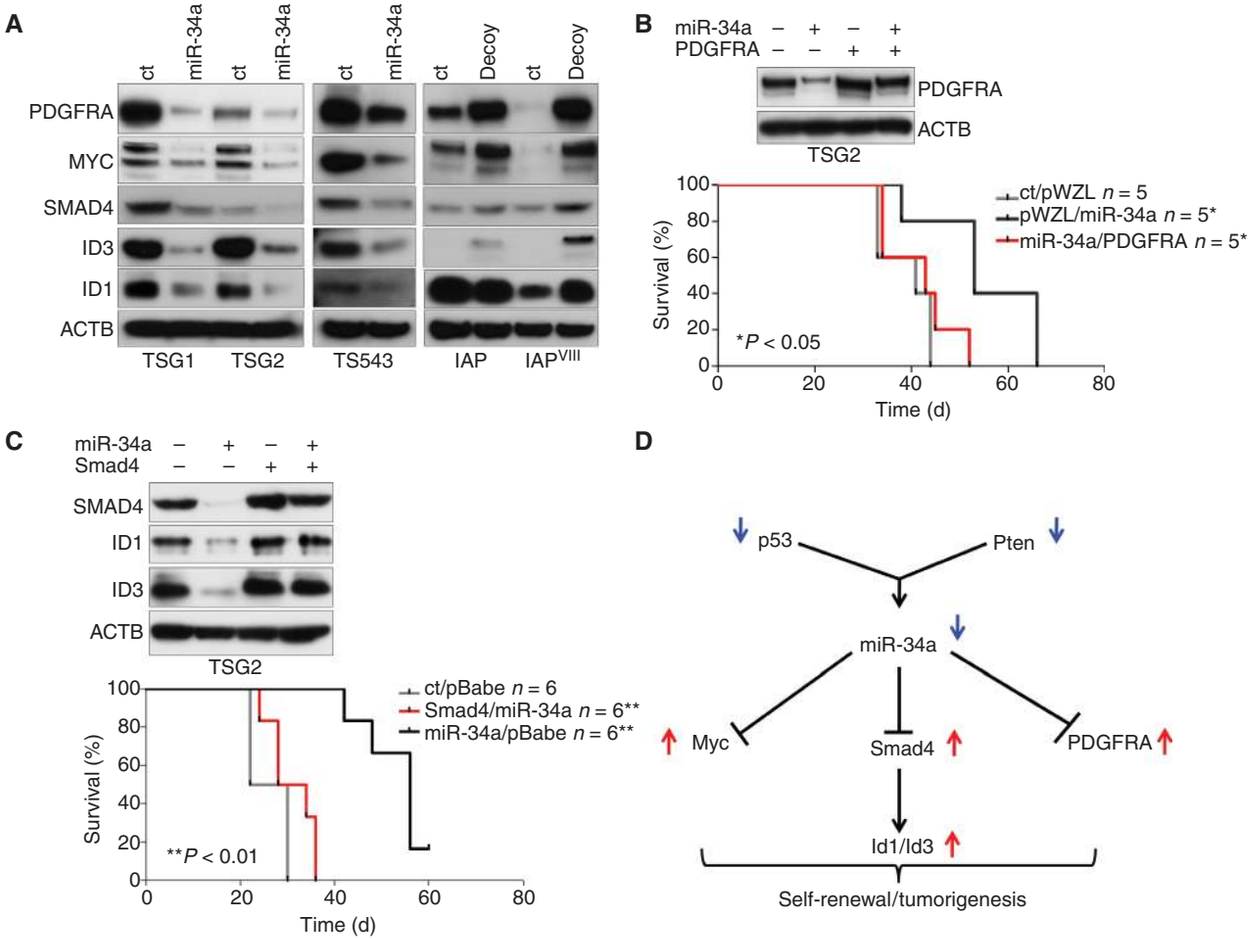

Figure 6. miR-34a functions through PDGFRA and ID proteins in proneural glioblastomas. **A,** expression levels of PDGFRA, MYC, SMAD4, ID1, and ID3 in response to miR-34a modulation, in mouse (TSG1/2) and human (TS543) proneural glioblastoma systems and in genetically engineered, immortalized mouse astrocytes (IAP and IAP^{VIII}). **B,** *in vivo* rescue experiments. Kaplan–Meier analysis of survival shows that murine *Pdgfra* rescues the antitumorigenic effects of miR-34a in *p53*/*Pten*$^{-/-}$ murine glioblastoma (TSG2) transplanted subcutaneously in Ncr/nude mice. Western blot analysis of protein expression in cells transduced with miR-34a, PDGFRA, and the appropriate controls. Protein levels were measured 72 hours after infection (top). **C,** *in vivo* rescue experiments. Kaplan–Meier analysis of survival shows that murine *Smad4* rescues the antitumorigenic effects of miR-34a in *p53*/*Pten*$^{-/-}$ murine glioblastoma (TSG2) transplanted subcutaneously in Ncr/nude mice. Western blot analysis of protein expression in cells transduced with miR-34a, *Smad4*, and the appropriate controls. Protein levels were measured 72 hours after the infection (top). **D,** a model showing a hierarchical subnetwork involving miR-34a and its upstream and downstream oncogenic nodes in proneural glioblastoma. IAP, *Ink4a*/*Arf*$^{-/-}$;*Pten*$^{-/-}$, IAP^{VIII}, *Ink4a*/*Arf*$^{-/-}$;*Pten*$^{-/-}$;*Egfr*$^{VIII/+}$.

(Fig. 6A) as well as in established human and mouse glioblastoma cells (Supplementary Fig. S9B). Conversely, decoy-based miR-34a knockdown in primary mouse astrocytes induced expression of PDGFRA (Fig. 6A), and reintroduction of the *Pdgfra* open reading frame was able to reverse the inhibition of tumorigenesis by miR-34a in the TSG2 system (Fig. 6B) as well as the spherogenic potential of mouse and human proneural malignant spheroids (Supplementary Fig. S10A–S10C, respectively). Together, these experimental data confirm that *PDGFRA* is a direct target of miR-34a that is functionally linked to proneural glioblastoma biology, consistent with a recent report (33).

miR-34a Regulates *TGF-β* Signaling via a *Smad4* Transcriptional Network

In line with the observation in the global CLR network, less than 1% of the miR-34a subnetwork (3 of the 342 nodes or 0.88%) was computationally predicted to be direct, suggesting that indirect mechanisms such as transcriptional regulation mediated through intermediate regulators, for example, transcription factors, may be at play (34). To identify such intermediates in the network, we conducted an *in silico* enrichment analysis for transcription factor–binding sites in promoter regions of mRNA nodes that are connected to miR-34a and defined as part of the proneural or mesenchymal signature (ref. 2; see Methods). Because miR-34a is strongly underexpressed in proneural samples, transcription factors that were (i) overrepresented in the binding sites of these proneural signature genes linked to miR-34a, (ii) overexpressed in proneural samples and exhibited (iii) a statistically significant negative correlation with miR-34a in the proneural subtype were defined as potential intermediaries through which miR-34a may act. This *in silico* analysis identified 3 transcription factors, *PBX1, SMAD4,* and *MYC,*

whose binding sites were significantly enriched ($P < 0.05$; Supplementary Table S10). While PBX1 was not expressed in either our human or mouse glioblastoma systems (data not shown), MYC has been shown to be a target regulated by miR-34a (ref. 35; data not shown) and is known to play a pivotal role in gliomagenesis in the *p53*/*Pten* GEM model of glioblastoma (28), thus providing support that the computational approach taken to identify transcription factor intermediates is biologically sound. With that, we next explored the putative relationship between miR-34a and *SMAD4*, a connection that has not been reported in any tumor type including glioblastoma.

Smad4 is a co-Smad required for R-Smad–mediated activation of *TGF-β* (transforming growth factor-β) signaling. A large body of literature has implicated critical roles for *TGF-β* signaling in cancers (36). In glioblastoma, the *TGF-β* pathway has been shown to act as an oncogenic factor (37), and *TGF-β* signaling can enhance self-renewal capacity of tumor-derived spheroids *in vitro*, an effect that is dependent on ID1 and ID3 (38). This gains significance in view of the observed effect of miR-34a on the spherogenic potency *in vitro*. Against this backdrop, the bioinformatic prediction of *SMAD4* as a putative transcription factor intermediate in the CLR network suggests that miR-34a may be a regulator of the TGF-β–SMAD–ID signaling pathway. Consistent with this is the observation of a strong negative correlation between expression of miR-34a and *SMAD4* in the TCGA data set (Supplementary Fig. S11). To functionally test this hypothesis, we examined the expression of SMAD4 and the ID family proteins in independent mouse (TSG1 and TSG2) and human (TS543) proneural-like glioblastoma tumor spheroid cultures in response to miR-34a. As shown in Fig. 6A, miR-34a downregulated SMAD4 and ID1/3 expression, and such regulation was through direct binding to a conserved consensus region in the 3′UTR of *SMAD4* based on the 3′UTR luciferase reporter assay (Supplementary Fig. S12). Conversely, in primary astrocytes, decoy sponging of endogenous miR-34a increased SMAD4 and ID1/3 expression (Fig. 6A). Next, to show a functional role of SMAD4 in the proneural system, we cotransduced *p53*/*Pten*$^{-/-}$ tumor spheroids cells with miR-34a and a *Smad4* expression vector to show that SMAD4 expression was sufficient to reverse the effect of miR-34a on ID1 and ID3 expression (Fig. 6C) and rescues its antitumorigenic activity both *in vitro* and *in vivo* (Fig. 6C; Supplementary Fig. S13). Overall our functional rescue studies suggest that in proneural glioblastoma, both PDGFRA and SMAD4 are key effectors downstream of miR-34a (Fig. 6D). Furthermore, as the activity of TGF-β on renewal of glioblastoma spheroid cultures has been reported to depend on ID1/ID3 expression (38), we showed that lentiviral-based hairpin knockdown of *Smad4*, *Id1*, or *Id3* in the mouse proneural-like system significantly reduced the number of spheroids when compared with the nontargeting control (Fig. 7A–D). Finally, we found that the stable knockdown of *Smad4* impairs tumorigenesis *in vivo* in intracranial transplants ($P < 0.01$; Fig. 7E), suggesting that the SMAD4–ID1–ID3 axis is crucial in regulating the homeostasis of malignant glioma cells in mouse proneural-like glioblastoma. In summary, mechanistic exploration guided by integrative analyses of transcription factor–binding site enrichment in context of this CLR-inferred network established a novel mechanism of action by miR-34a whereby it exerts its diverse transcriptomic influences through the modulation of the TGF-β transcriptomic network through the direct binding of the *SMAD4* 3′UTR.

DISCUSSION

Glioblastoma is a heterogeneous disease characterized by distinct molecular subtypes underlying different biologic behaviors and response to therapies. Leveraging the multidimensional TCGA data set, reverse-engineering with the CLR algorithm has provided an inferred map of the putative miR–mRNA regulatory network in glioblastoma. Integrating this network model with molecular subtype definition and functional genomic screen, as well as *in silico* sequence-based target prediction and promoter analysis, we prioritized miR-34a for downstream mechanistic studies. These studies uncovered a novel regulatory network emanating from miR-34a, which acts as a tumor suppressor in proneural-like glioblastoma, in part, through direct action on *PDGFR*A as recently shown by Silber and colleagues (33) in addition to commandeering of the *SMAD4* transcriptomic network to regulate ID1 and ID3 levels. That the majority of mRNAs computed to link to a miR node appears to be regulated indirectly through transcription factors, such as SMAD4 (this study) and MYC (35, 39) likely serves as an amplifier of an effect of miR on the global transcriptome. This finding thus provides a rationale for an alternative approach to inhibit transcription factor activity through modulating its upstream miR regulatory node. In sum, this work illustrates not only the power of comprehensive cancer genomic data sets such as that of TCGA and the importance of mining and interpreting such data sets in the context of cancer biology but also the value of computational and experimental models in enabling an understanding of the underlying complexity of the disease.

Although miR-34a has been implicated in multiple cancer types (40), its roles in the regulation of SMAD4–ID1–ID3 have not been previously suggested. While the relationship between *PDGFRA* and miR-34a is predicted by sequence-based algorithms, the relationship between miR-34a and SMAD4 or its downstream ID1 and ID3 are not; therefore, the hypothesis that they could be mediators of miR-34a activity came only through unbiased analysis for transcription factor–binding site enrichment in the promoters of CLR-inferred mRNA nodes linked to miR-34a. This reinforces the power of global systembiology approaches in generating unanticipated hypotheses.

Equally important are appropriate experimental models that enable genetic (or pharmacologic) perturbations to examine the validity of network connections inferred by the computational models. The importance of the GEM model of proneural-like glioblastoma is of particular relevance, as most of the well-established human glioblastoma cell models or human tumor spheroid cultures do not represent the proneural subtype; indeed, using this system, we show that miR-34a exerts its tumor-suppressive function by impinging on self-renewal through the TGF-β/SMAD pathway (38). The ability to show the relationship of miR-34a with PDGFRA and SMAD4–ID nuclear oncoproteins in spontaneous *de novo* glioblastoma in *p53*/*Pten*$^{-/-}$ GEM model, and the effects of the experimental perturbation of these oncogenic axes on cancer cell homeostasis in this system provide strong evidence that

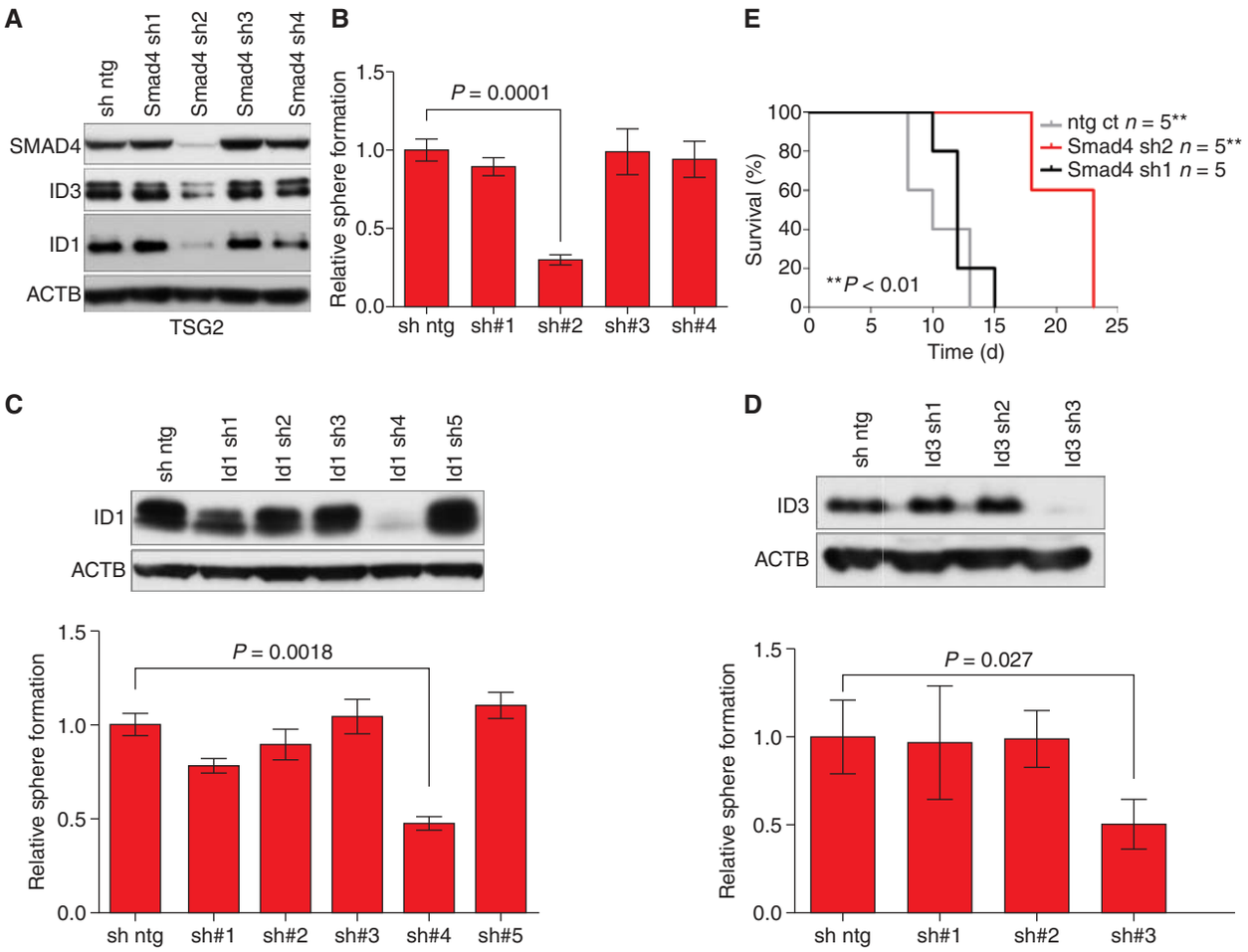

Figure 7. The functional inactivation of SMAD4 and ID proteins impairs tumorigenesis and self-renewal in proneural glioblastoma. **A,** Western blot analysis of SMAD4, ID1, and ID3 proteins 72 hours after infecting *p53/Pten*$^{-/-}$ glioma cells (TSG2) with short hairpin RNA (shRNA) constructs specific for murine *Smad4*. **B,** stable knockdown of *Smad4* by lentiviral shRNA impairs the self-renewal capacity of mouse proneural spheroids (TSG2) *in vitro*. Error bars represent SD of experimental triplicates. **C,** stable knockdown of *Id1* by lentiviral shRNA impairs the self-renewal capacity of mouse proneural spheroids (TSG2) *in vitro*. Protein levels were measured 72 hours after the infection (top). Error bars represent SD of experimental triplicates. **D,** stable knockdown of *Id3* by lentiviral shRNA impairs the self-renewal capacity of mouse proneural-like spheroids (TSG2) *in vitro*. Protein levels were measured 72 hours after the infection (top). Error bars represent SD of experimental triplicates. **E,** Kaplan–Meier survival analysis of Ncr/nude mice transplanted orthotopically with *p53/Pten*$^{-/-}$ murine glioblastoma cells harboring hairpins specific for murine *Smad4* (sh1 and sh2) or the vector control (ntg ct).

the predicted regulatory relationships are relevant and operative *in vivo* in an intact microenvironment.

Finally, our findings in this study have potential clinical application, as miR-34a expression level is shown in 2 independent cohorts of glioblastoma to stratify patients into good and poor prognosis subgroups with significant difference in overall survival. Furthermore, within the TCGA cohort, we found that miR-34a carries significant overlap in prognostic significance with glioma-CpG island methylator phenotype (G-CIMP) status (ref. 5; data not shown), suggesting a possible mechanistic relationship between miR-34a and G-CIMP, although elucidation of the molecular basis for this relationship will require further studies.

Previous studies have reported miR-34a expression level as a prognostic parameter. For instance, in pancreatic ductal adenocarcinoma, miR-34a loss (i.e., low to no expression) is associated with a decreased survival probability (41); in other words, miR-34a–expressing pancreatic ductal adenocarcinoma has a relatively better survival. In breast cancer, although high miR-34a expression is correlated with poor prognosis factors including positive nodal status, high tumor grade, estrogen receptor negativity, HER2 positivity, and high proliferation rate, after adjusting for these known prognostic parameters in multivariant analysis, high miR-34a expression is in fact associated with a lower risk of recurrence or death from breast cancer (42), indicating that high levels of miR-34a are a good prognostic factor. In contrast to these previous studies, our analyses of 2 independent cohorts of glioblastoma showed that miR-34a low-expressing glioblastomas have better outcome with longer overall survival. In other words, glioblastoma tumors driven by inactivation of miR-34a are less aggressive than glioblastomas that evolve through deregulation of other genetic elements. The differences in prognostic significance of miR-34a loss in different tumor types likely reflect the modulatory effects of preexisting genetic alterations and the specific susceptibility of different cell types to the aberrant activation of any given

pathway. This is not dissimilar to the case of another glioma gene, *IDH1*, whose specific point mutation affecting a key residue in the protein (R132) has been shown to be oncogenic. Interestingly, gliomas carrying this mutation in *IDH1* as well as analogous mutations affecting *IDH2* have a significantly better prognosis (43–46). On the other hand, in cytogenetically normal acute myelogenous leukemia carrying *NPM1* mutations, IDH1 mutations at the same residue are a poor prognostic factor as patients with IDH1 mutations do worse (47, 48). In summary, we illustrate here that computational network modeling of the complex interrelationships among diverse genetic elements can generate a logical framework in which to explore and understand the genetics and biology of cancers, and when integrated with disease knowledge and clinical annotation can lead to discovery of new pathogenetic insights in addition to potential prognostic biomarkers or therapeutic targets. In this regard, we believe that the results from this study should motivate future efforts to explore the therapeutic implication of miR-34a reconstitution. The potent tumor-suppressive activity in our preclinical models would suggest possible therapeutic benefit of miR-34a reconstitution by tumor-targeted delivery in low miR-34a–expressing glioblastoma. In view of its mechanism of action through PDGFRA, MYC, and SMAD4, one may further speculate that reconstitution of miR-34a could represent an attractive strategy to deliver combination therapy against multiple *bona fide* cancer gene targets.

METHODS

Bioinformatic Analysis

Network inference was conducted, both globally and within each of the 4 molecular subtype sample sets, using the CLR algorithm on 290 matched miR and mRNA expression profiles from the TCGA. Copy number analysis was conducted on level 3 segmented data by the CN Tools Bioconductor package using 90th percentile segment gain or loss (SGOL) values as thresholds. Gene weight analysis was done to test for correlation of expression and copy number change for each miR and mRNA species. Transcription factor motifs were identified on the basis of coincidental prediction of binding sites by the CisGenome and MotifScanner programs in promoter regions (−8 kb, +2 kb of transcription start site).

Mouse and Human Proneural Glioblastoma Cell Lines

p53$^{L/L}$;Pten$^{L/+}$;Gfap-Cre and *p53$^{L/L}$;Pten$^{L/L}$; Gfap-Cre* mice have been previously described (28). Primary murine astrocytes were isolated from *Gfap-Cre;Ink4a/Arf$^{L/L}$;Pten$^{L/L}$* and *Gfap-Cre;Ink4a/Arf$^{L/L}$;Pten$^{L/L}$; EgfrLSL$^{VIII/+}$*. GEM models were provided by Ronald A. DePinho. Murine cell lines were created by enzymatic and mechanical dissociation of individual samples, all genotypes were verified by PCR amplification of genomic DNA and gel electrophoresis. The Harvard Institutional Animal Care and Use Committee approved all animal studies and procedures. TS543 human malignant spheroids are short-term cultures derived from a primary proneural glioblastoma kindly provided by C. Brennan. PDGFRA expression was validated by Western blot analysis.

An extensive description of the materials and methods is provided in the Supplementary Information.

Disclosure of Potential Conflicts of Interest

D.L. Rimm is a consultant to and stockholder in HistoRx, the exclusive licensee of the AQUA patent. No potential conflicts of interest were disclosed by the other authors.

Authors' Contributions

Conception and design: G. Genovese, S. Sarkar, J. Zhang, J.J. Collins, L. Chin

Development of methodology: G. Genovese, A. Ergun, S.A. Shukla, J. Hanna, S. Colla, S. Sarkar, J. Zhang, D.L. Rimm, J.J. Collins, L. Chin

Acquisition of data (provided animals, acquired and managed patients, provided facilities, etc.): G. Genovese, B. Campos, J. Hanna, P. Ghosh, S.N. Quayle, K. Rai, S. Colla, H. Ying, H. Zhang, K. Dunn, C. Brennan, H. Zheng, D.L. Rimm

Analysis and interpretation of data (e.g., statistical analysis, biostatistics, computational analysis): G. Genovese, A. Ergun, S.A. Shukla, B. Campos, P. Ghosh, S.N. Quayle, K. Rai, C.-J. Wu, S. Sarkar, Y. Xiao, J. Zhang, H. Zhang, L. Kwong, C. Brennan, D.L. Rimm, L. Chin

Writing, review, and/or revision of the manuscript: G. Genovese, A. Ergun, S.A. Shukla, B. Campos, J. Hanna, C.-J. Wu, S. Sarkar, D.L. Rimm, J.J. Collins, L. Chin

Administrative, technical, or material support (i.e., reporting or organizing data, constructing databases): W.R. Wiedemeyer, L. Chin

Study supervision: J.J. Collins, L. Chin

Formulated overall approaches for analysis and identification of most discriminatory miRs: A. Ergun, S.A. Shukla

Network inference modeling and integration with copy number data: A. Ergun

Conducted gene set enrichment, direct target prediction results, and promoter analyses: S.A. Shukla

Conducted correlation of copy number with expression analysis: J. Zhang, H. Zhang

Generated and analyzed the tissue microarray data: B. Campos, J. Hanna, D.L. Rimm

Conducted the survival analysis: C.-J. Wu

Conducted *in vivo* experiments: G. Genovese, P. Ghosh, H. Ying

Established the lentiviral vector systems: G. Genovese, S. Colla

Conducted luciferase reporter assays: S.N. Quayle

Conducted *in vitro* studies: B. Campos, K. Rai, S. Sarkar, K. Dunn

Conducted signaling analysis: W.R. Wiedemeyer

Analyzed microarray data: L. Kwong

Acknowledgments

The authors thank the support of the Belfer Institute for Applied Cancer Science for computational analyses; Drs. Ronald A. DePinho, Giulio Draetta, and members of the Chin laboratories; Alessandro Sgambato and Stefano Sioletic for comments and reagents; Joshua Mendell for the MSCV-PIG miR-34a construct; and Zhou Shan, Jiang Shan, and Carla Bianchi for mouse husbandry and colony care. All the expression clones were obtained through the Dana Farber/Harvard Plasmid Core Facility. The pHage vector was originally developed by Darrel Kotton. Human glioma spheroids were provided by C. Brennan. GEM models and immortalized human astrocytes with the E6/E7 oncoproteins and Tert were provided by Ronald A. DePinho.

Grant Support

This work is supported by funding from the NIH (PO1 CA095616, U01 CA141508, and U24 CA143845) and from the Ben and Catherine Ivy Foundation to L. Chin. J.J. Collins is an HHMI investigator. G. Genovese was supported by the AIRC "Associazione Italiana per la Ricerca sul Cancro" fellowship. S.A. Shukla was supported by The Robert A. and Renee E. Belfer foundation and by the GDAC grant (NIH U24 CA143845). P. Ghosh was supported by a NIH F32 fellowship. S.N. Quayle was supported by a fellowship from the Canadian Institutes of Health Research. K. Rai was supported by an NIH K99/R00 Pathway to Independence award (1K99CA160578-01) and Charles A. King Trust postdoctoral fellowship. K. Dunn was supported by the Terry Fox Foundation (#2009-700118). S. Sarkar

was supported by a fellowship from the Ovarian Cancer Research Foundation. C. Brennan is supported by the NIH P01 CA95616 grant.

Received March 13, 2012; revised June 18, 2012; accepted June 20, 2012; published OnlineFirst June 29, 2012.

REFERENCES

1. Furnari FB, Fenton T, Bachoo RM, Mukasa A, Stommel JM, Stegh A, et al. Malignant astrocytic glioma: genetics, biology, and paths to treatment. Genes Dev 2007;21:2683–710.
2. Verhaak RG, Hoadley KA, Purdom E, Wang V, Qi Y, Wilkerson MD, et al. Integrated genomic analysis identifies clinically relevant subtypes of glioblastoma characterized by abnormalities in PDGFRA, IDH1, EGFR, and NF1. Cancer Cell 2010;17:98–110.
3. Phillips HS, Kharbanda S, Chen R, Forrest WF, Soriano RH, Wu TD, et al. Molecular subclasses of high-grade glioma predict prognosis, delineate a pattern of disease progression, and resemble stages in neurogenesis. Cancer Cell 2006;9:157–73.
4. Brennan C, Momota H, Hambardzumyan D, Ozawa T, Tandon A, Pedraza A, et al. Glioblastoma subclasses can be defined by activity among signal transduction pathways and associated genomic alterations. PLoS One 2009;4:e7752.
5. Noushmehr H, Weisenberger DJ, Diefes K, Phillips HS, Pujara K, Berman BP, et al. Identification of a CpG island methylator phenotype that defines a distinct subgroup of glioma. Cancer Cell 2010;17:510–22.
6. Bartel DP. MicroRNAs: genomics, biogenesis, mechanism, and function. Cell 2004;116:281–97.
7. Krol J, Loedige I, Filipowicz W. The widespread regulation of microRNA biogenesis, function and decay. Nat Rev Genet 2010;11:597–610.
8. Calin GA, Sevignani C, Dumitru CD, Hyslop T, Noch E, Yendamuri S, et al. Human microRNA genes are frequently located at fragile sites and genomic regions involved in cancers. Proc Natl Acad Sci U S A 2004;101:2999–3004.
9. Calin GA, Ferracin M, Cimmino A, Di Leva G, Shimizu M, Wojcik SE, et al. A MicroRNA signature associated with prognosis and progression in chronic lymphocytic leukemia. N Engl J Med 2005;353:1793–801.
10. Lu J, Getz G, Miska EA, Alvarez-Saavedra E, Lamb J, Peck D, et al. MicroRNA expression profiles classify human cancers. Nature 2005;435:834–8.
11. He L, Thomson JM, Hemann MT, Hernando-Monge E, Mu D, Goodson S, et al. A microRNA polycistron as a potential human oncogene. Nature 2005;435:828–33.
12. Croce CM. Causes and consequences of microRNA dysregulation in cancer. Nat Rev Genet 2009;10:704–14.
13. Sumazin P, Yang X, Chiu HS, Chung WJ, Iyer A, Llobet-Navas D, et al. An extensive microRNA-mediated network of RNA-RNA interactions regulates established oncogenic pathways in glioblastoma. Cell 2011;147:370–81.
14. Karreth FA, Tay Y, Perna D, Ala U, Tan SM, Rust AG, et al. *In vivo* identification of tumor-suppressive PTEN ceRNAs in an oncogenic BRAF-induced mouse model of melanoma. Cell 2011;147:382–95.
15. Tay Y, Kats L, Salmena L, Weiss D, Tan SM, Ala U, et al. Coding-independent regulation of the tumor suppressor PTEN by competing endogenous mRNAs. Cell 2011;147:344–57.
16. Su WL, Kleinhanz RR, Schadt EE. Characterizing the role of miRNAs within gene regulatory networks using integrative genomics techniques. Mol Syst Biol 2011;7:490.
17. Dong H, Luo L, Hong S, Siu H, Xiao Y, Jin L, et al. Integrated analysis of mutations, miRNA and mRNA expression in glioblastoma. BMC Syst Biol 2010;4:163.
18. Mestdagh P, Lefever S, Pattyn F, Ridzon D, Fredlund E, Fieuw A, et al. The microRNA body map: dissecting microRNA function through integrative genomics. Nucleic Acids Res 2011;39(Database issue):e136.
19. Grigoryev YA, Kurian SM, Hart T, Nakorchevsky AA, Chen C, Campbell D, et al. MicroRNA regulation of molecular networks mapped by global microRNA, mRNA, and protein expression in activated T lymphocytes. J Immunol 2011;187:2233–43.
20. Sharbati J, Lewin A, Kutz-Lohroff B, Kamal E, Einspanier R, Sharbati S. Integrated microRNA-mRNA-analysis of human monocyte derived macrophages upon Mycobacterium avium subsp. hominissuis infection. PLoS One 2011;6:e20258.
21. Faith JJ, Hayete B, Thaden JT, Mogno I, Wierzbowski J, Cottarel G, et al. Large-scale mapping and validation of *Escherichia coli* transcriptional regulation from a compendium of expression profiles. PLoS Biol 2007;5:e8.
22. Cancer Genome Atlas Research Network. Comprehensive genomic characterization defines human glioblastoma genes and core pathways. Nature 2008;455:1061–8.
23. Chen K, Rajewsky N. Natural selection on human microRNA binding sites inferred from SNP data. Nat Genet 2006;38:1452–6.
24. Grimson A, Farh KK, Johnston WK, Garrett-Engele P, Lim LP, Bartel DP. MicroRNA targeting specificity in mammals: determinants beyond seed pairing. Mol Cell 2007;27:91–105.
25. Krek A, Grun D, Poy MN, Wolf R, Rosenberg L, Epstein EJ, et al. Combinatorial microRNA target predictions. Nat Genet 2005;37:495–500.
26. Lewis BP, Burge CB, Bartel DP. Conserved seed pairing, often flanked by adenosines, indicates that thousands of human genes are microRNA targets. Cell 2005;120:15–20.
27. Betel D, Wilson M, Gabow A, Marks DS, Sander C. The microRNA.org resource: targets and expression. Nucleic Acids Res 2008;36:D149–53.
28. Zheng H, Ying H, Yan H, Kimmelman AC, Hiller DJ, Chen AJ, et al. p53 and Pten control neural and glioma stem/progenitor cell renewal and differentiation. Nature 2008;455:1129–33.
29. Kim SY, Volsky DJ. PAGE: parametric analysis of gene set enrichment. BMC Bioinformatics 2005;6:144.
30. Li Y, Guessous F, Zhang Y, Dipierro C, Kefas B, Johnson E, et al. MicroRNA-34a inhibits glioblastoma growth by targeting multiple oncogenes. Cancer Res 2009;69:7569–76.
31. He L, He X, Lim LP, de Stanchina E, Xuan Z, Liang Y, et al. A microRNA component of the p53 tumour suppressor network. Nature 2007;447:1130–4.
32. Gentner B, Schira G, Giustacchini A, Amendola M, Brown BD, Ponzoni M, et al. Stable knockdown of microRNA in vivo by lentiviral vectors. Nat Methods 2009;6:63–6.
33. Silber J, Jacobsen A, Ozawa T, Harinath G, Pedraza A, Sander C, et al. miR-34a repression in proneural malignant gliomas upregulates expression of its target PDGFRA and promotes tumorigenesis. PLoS One 2012;7:e33844.
34. Carro MS, Lim WK, Alvarez MJ, Bollo RJ, Zhao X, Snyder EY, et al. The transcriptional network for mesenchymal transformation of brain tumours. Nature 2010;463:318–25.
35. Christoffersen NR, Shalgi R, Frankel LB, Leucci E, Lees M, Klausen M, et al. p53-independent upregulation of miR-34a during oncogene-induced senescence represses MYC. Cell Death Differ 2010;17:236–45.
36. Ikushima H, Miyazono K. TGFbeta signalling: a complex web in cancer progression. Nat Rev Cancer 2010;10:415–24.
37. Massague J. TGFbeta in cancer. Cell 2008;134:215–30.
38. Anido J, Saez-Borderias A, Gonzalez-Junca A, Rodon L, Folch G, Carmona MA, et al. TGF-beta receptor inhibitors target the CD44(high)/Id1(high) glioma-initiating cell population in human glioblastoma. Cancer cell 2010;18:655–68.
39. Choi YJ, Lin CP, Ho JJ, He X, Okada N, Bu P, et al. miR-34 miRNAs provide a barrier for somatic cell reprogramming. Nat Cell Biol 2011;13:1353–60.
40. Hermeking H. The miR-34 family in cancer and apoptosis. Cell Death Differ 2010;17:193–9.
41. Jamieson NB, Morran DC, Morton JP, Ali A, Dickson EJ, Carter R, et al. MicroRNA molecular profiles associated with diagnosis,

clinicopathological criteria, and overall survival in patients with resectable pancreatic ductal adenocarcinoma. Clin Cancer Res 2012;18:534–45.
42. Peurala H, Greco D, Heikkinen T, Kaur S, Bartkova J, Jamshidi M, et al. MiR-34a expression has an effect for lower risk of metastasis and associates with expression patterns predicting clinical outcome in breast cancer. PLoS One 2011;6:e26122.
43. Lu C, Ward PS, Kapoor GS, Rohle D, Turcan S, Abdel-Wahab O, et al. IDH mutation impairs histone demethylation and results in a block to cell differentiation. Nature 2012;483:474–8.
44. Parsons DW, Jones S, Zhang X, Lin JC, Leary RJ, Angenendt P, et al. An integrated genomic analysis of human glioblastoma multiforme. Science 2008;321:1807–12.
45. Yan H, Parsons DW, Jin G, McLendon R, Rasheed BA, Yuan W, et al. IDH1 and IDH2 mutations in gliomas. N Engl J Med 2009;360:765–73.
46. Koivunen P, Lee S, Duncan CG, Lopez G, Lu G, Ramkissoon S, et al. Transformation by the (R)-enantiomer of 2-hydroxyglutarate linked to EGLN activation. Nature 2012;483:484–8.
47. Marcucci G, Maharry K, Wu YZ, Radmacher MD, Mrozek K, Margeson D, et al. IDH1 and IDH2 gene mutations identify novel molecular subsets within *de novo* cytogenetically normal acute myeloid leukemia: a Cancer and Leukemia Group B study. J Clin Oncol 2010;28:2348–55.
48. Paschka P, Schlenk RF, Gaidzik VI, Habdank M, Kronke J, Bullinger L, et al. IDH1 and IDH2 mutations are frequent genetic alterations in acute myeloid leukemia and confer adverse prognosis in cytogenetically normal acute myeloid leukemia with NPM1 mutation without FLT3 internal tandem duplication. J Clin Oncol 2010;28:3636–43.